

## Two-Dimensional Mapping of the Central and Parafoveal Visual Field to Human Visual Cortex

Mark M. Schira, Alex R. Wade, and Christopher W. Tyler

Smith-Kettlewell Eye Research Institute, San Francisco, California

Submitted 11 September 2006; accepted in final form 1 March 2007

**Schira MM, Wade AR, Tyler CW.** Two-dimensional mapping of the central and parafoveal visual field to human visual cortex. *J Neurophysiol* 97: 4284–4295, 2007. First published March 14, 2007; doi:10.1152/jn.00972.2006. Primate visual cortex contains a set of maps of visual space. These maps are fundamental to early visual processing, yet their form is not fully understood in humans. This is especially true for the central and most important part of the visual field—the fovea. We used functional magnetic resonance imaging (fMRI) to measure the mapping geometry of human V1 and V2 down to 0.5° of eccentricity. By applying automated atlas fitting procedures to parametrize and average retinotopic measurements of eight brains, we provide a reference standard for the two-dimensional geometry of human early visual cortex of unprecedented precision and analyze this high-quality mean dataset with respect to the 2-dimensional cortical magnification morphometry. The analysis indicates that 1) area V1 has meridional isotropy in areal projection: equal areas of visual space are mapped to equal areas of cortex at any given eccentricity. 2) V1 has a systematic pattern of local anisotropies: cortical magnification varies between isopolar and isoeccentricity lines, and 3) the shape of V1 deviates systematically from the complex-log model, the fit of which is particularly poor close to the fovea. We therefore propose that human V1 be fitted by models based on an equal-area principle of its two-dimensional magnification. 4) V2 is elongated by a factor of 2 in eccentricity direction relative to V1 and has significantly more local anisotropy. We propose that V2 has systematic intrinsic curvature, but V1 is intrinsically flat.

### INTRODUCTION

Human primary visual cortex (V1) contains a map of visual space: to a good approximation, each two-dimensional (2D) location in the visual field is represented at a single physical location within V1 (Hubel and Wiesel 1974). This mapping was first studied in human by Inouye (1909), and subsequent work (Holmes 1917; Horton and Hoyt 1991a,b) refined our understanding of the way that the visual world is represented in early visual cortex. Early behavioral studies (Wertheim 1894) and anatomical examination of the retina (Curcio et al. 1990; Østerberg 1935) showed that the fovea is a region of high spatial acuity. It is therefore not unexpected that the visual system allocates proportionally more gray matter to the representation of the fovea. This “cortical magnification” was quantified in the monkey by Talbot and Marshall (1941) and in more detail by Daniel and Whitteridge (1961). Subsequent studies (Dow et al. 1981–1985; Levi et al. 1984; Van Essen et al. 1984; Yap et al. 1987) have improved our estimates of this function, which describes the way that linear magnification changes with ec-

centricity. Magnification (in mm displacement on the cortex / ° in the visual field) is often described by the function:

$$M(E) = \frac{k}{E + a}. \quad (1)$$

In this notation, magnification  $M$  depends on eccentricity ( $E$ ) but not angular (“polar”) position (which we will denote as  $P$ ) in the visual field. In fact, linear magnification can be measured parallel to isopolar lines ( $M_P$ ) or parallel to isoeccentricity lines ( $M_E$ ) and in general,  $M_E$  and  $M_P$  are not equal. The product of these two metrics is  $M_A$  or the “areal magnification” (Myerson et al. 1977; Tusa et al. 1978): the area of cortical surface (in mm<sup>2</sup>) per area of visual field (in deg<sup>2</sup>). The distinctions among these metrics are important in this paper and we provide a detailed analysis in the APPENDIX.

In 1977, Schwartz proposed an analytical expression to describe the 2D mapping between retinal and cortical coordinates. By using complex numbers to represent both retinal eccentricity and angular deviation from the horizontal meridian simultaneously, he showed that the map of visual space in area V1 symbolized by  $w(E, P)$ , was approximated by a complex-log transform of the retinal image (Schwartz 1977).

$$w(E, P) = k * \log(E * e^{iP} + a), \quad (2)$$

where  $a$  defines the extent of the foveal singularity and  $k$  is a scaling constant.

This simple and convenient complex-log transform (or variants thereof—Balasubramanian et al. 2002; Polemeni et al. 2006; Schwartz 1983) captures several important features of the V1 map—most notably the roughly logarithmic scaling of cortical area with eccentricity. It has become the de facto standard for describing the shape of human V1. However, the complex-log representation makes some counterintuitive predictions about the way that space is represented in visual cortex (see APPENDIX). Specifically, the log-polar transform of Eq. 2 requires that the amount of cortex dedicated to a particular area of visual space varies with polar angle as well as eccentricity. There is no a priori reason for believing that this is the case, and in fact, behavioral studies show that psychophysical properties that might be expected to depend on local cortical area (for example Vernier acuity or contrast sensitivity) are essentially independent of angular position in the visual field (Rovamo and Virsu 1984; Toet and Levi 1992).

We term a change in cortical magnification with polar position but constant eccentricity *meridional anisotropy* to

Address for reprint requests and other correspondence: M. M. Schira, The Smith-Kettlewell Eye Research Institute, 2318 Fillmore St., San Francisco, CA 94115 (E-mail: mark@ski.org).

The costs of publication of this article were defrayed in part by the payment of page charges. The article must therefore be hereby marked “advertisement” in accordance with 18 U.S.C. Section 1734 solely to indicate this fact.

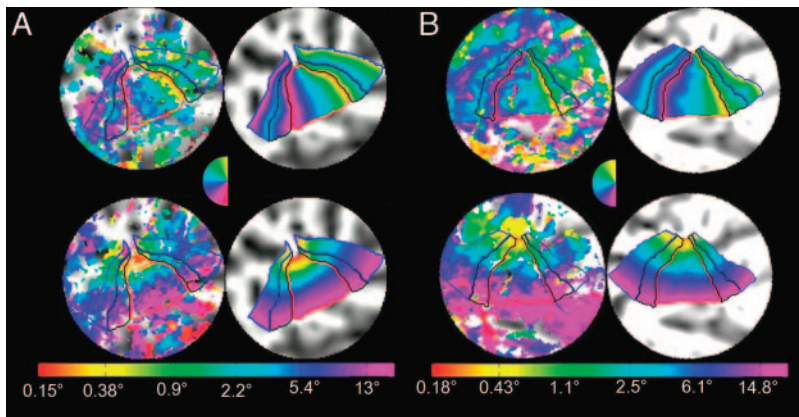


FIG. 1. *A* and *B*: ATLAS fits in 2 subjects shown on flattened representations of visual cortex. *Top row*: measurements of angular position (semi-circular wedge icons); *bottom row*: measurements of visual field eccentricity (eccentricity bar). In each pair of maps, the original functional magnetic resonance imaging (fMRI) data are on the left and the resulting atlas fits are on the right. Visual areas V1–V3 are indicated by red, black, and blue borders, respectively. It is important to emphasize that, although these data are displayed most conveniently on flattened cortical sheets, all our measurements were made within the original, folded cortical manifold to avoid distortion.

distinguish it from local anisotropies (see APPENDIX), following previous work (Buchanan-Smith and Heeley 1993; Mitchell et al. 1967; Westheimer 2003). It has also been termed “radial bias” (Fiorani et al. 1989; Van Essen et al. 1984).

Since the mid-1990s, researchers have used functional magnetic resonance imaging (fMRI) to measure the mapping of the visual field in the cerebral cortex. Early studies (DeYoe et al. 1996; Engel 1995; Sereno et al. 1995) demonstrated that it was possible to distinguish the “first tier” retinotopic visual areas (V1–V3). More recent work has focused on measuring the linear (1-dimensional) cortical magnification function (Duncan and Boynton 2003; Sereno 1995) or the area of cortex associated with different eccentricity ranges (Dougherty et al. 2003). However, none of these studies has quantified the 2-dimensional shape or the dependence on polar position.

Measuring the shape of V1 in the fovea is critical for several reasons. First the fovea is represented by a disproportionately large amount of cortex. Although the visual field extends over almost 180° of visual angle, approximately 30% of V1 is devoted to the central 3°. Second, the fovea supports a large proportion of functional vision: it is the location where visual acuity and color discrimination are highest, and many visual functions such as object and face identification, stereopsis and reading are essentially limited to the central visual field (Battista et al. 2005; Zegarra-Moran and Geiger 1993). Finally, as we show in this study, different models of retino-cortical mapping can make similar predictions in the periphery but very different predictions near the fovea depending on the strategy adopted to avoid the singularity at zero degrees eccentricity. If a simple analytical expression for the mapping between visual space and cortical location can be found, it is most strongly constrained (and most effectively tested) in the fovea. Conversely, incorrect models produce the most extreme errors in this region.

In the present study, we used high-resolution fMRI to measure the shape and morphometry of V1 and V2 to within 0.5° of the center of the visual field. This allowed us to model the way in which the amount of cortical area dedicated to a particular region of the visual field changes with both polar angle and eccentricity. We used an atlas fitting procedure to determine the retinotopic map in V1–V3 semi-automatically and made detailed local measurements of all the intrinsic distances between arrays of points in the V1 and V2 maps. We then averaged the metric data from eight observers to generate a “mean” V1 morphometry that strongly constrained our subsequent modeling. Our results indicate that the standard complex-log transform does not adequately describe the way in

which visual space is mapped to cortex. In particular, we find that this model overestimates the dependence of  $M_A$  on polar angle near the fovea. We show that a modified version of the complex-log transform provides a good fit to the measured data, and we suggest an analytic mapping function as a useful way to describe the transformation between 2D visual space and cortex. Our new model also provides a good approximation of human V2 and suggests detailed hypotheses about differences between V1 and V2.

#### METHODS

We analyzed retinotopic measurements from eight subjects, five male and three female, ranging in age from 25 to 60. Protocols were approved by the Institute Institutional Review Boards of both the Stanford and the Smith-Kettlewell Eye Research Institute, and informed consent was obtained from all subjects. Their vision was normal or corrected to normal for the stimulus presentation in the scanner.

#### Functional measurements

Functional magnetic resonance data were acquired on a GE 3T Signa LX scanner (GE Medical Systems, Milwaukee, WI) using a custom-built high-gain head coil. Functional acquisition was taken with a resolution of either  $2 \times 2 \times 3$  or  $2.5 \times 2.5 \times 3$  mm, using a spiral K-space sampling sequence of the T2\*-weighted (TE: 30 ms, 2 interleaves, 70° flip angle) activation (Noll et al. 1995) with 21 or 30 slices perpendicular to the calcarine sulcus, and a volume repetition time (TR) of 3 s. Subjects’ heads were fixed throughout the measurement period by means of snug-fitting pads and tape across the chin and forehead.

#### Anatomical measurements

Several high-resolution T1 datasets ( $1 \times 1 \times 1$  mm) were acquired for each subject using a fast three-dimensional (3D) SPGR sequence. These datasets were corrected for inhomogeneity, aligned, and averaged using the FMRIB software library (<http://www.fmrib.ox.ac.uk/fsl>) and SPM (<http://www.fil.ion.ucl.ac.uk/spm/>) to generate low-noise, spatially homogeneous datasets. Segmentation was performed using mrGray software package (<http://white.stanford.edu/~brian/mri/segmentUnfold.htm>), and each white-matter segmentation was carefully hand-edited to ensure an accurate segmentation and surface reconstruction.

#### Stimulus generation and presentation

Rotating wedges and expanding rings containing 4-Hz contrast-reversing checkerboard stimuli were generated using custom software

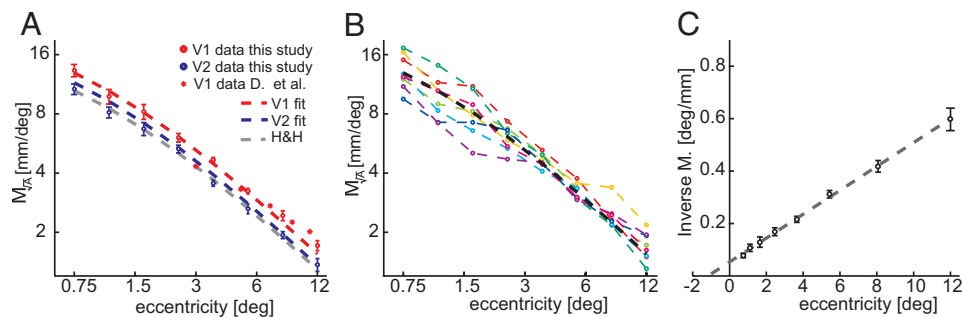


FIG. 2. Mean  $M_{VA}$  vs. eccentricity across all subjects fitted by Eq. 1. *A*: measurements across areas and studies. V1 data are plotted in red (fit:  $a = 0.77 \pm 0.03$ ;  $k = 19.2 \pm 0.25$ ) and V2 data are plotted in blue (fit:  $a = 0.73 \pm 0.03$ ;  $k = 15.9 \pm 0.21$ ). The gray line shows the cortical magnification function (V1) from Horton and Hoyt (1991a) ( $a = 0.75$ ;  $k = 17.6$ ) and the red \* symbols are points from Dougherty et al. (2003), error bars depict SE. Because our measurements did not extend beyond  $12^\circ$  of eccentricity, the data are well described by the monopole model or the corresponding linear magnification function (Eq. 1). *B*: individual measurements from the present study. Colored graphs show the results on individual subjects, the dotted gray line the fit for V1. *C*: mean inverse magnification of V1 with the best-fitting straight line for ready comparison with studies such as Rovamo and Virsu (1979), Levi et al. (1984), McKee and Nakayama (1984), Stensaas et al. (2001), Tyler (2001), and Duncan and Boynton (2003).

and routines from the Psychophysics Toolbox (Brainard 1997; Pelli 1997). To ensure good fixation, an extended fixation grid was present throughout the stimulus presentations (Tyler et al. 2005). The fixation grid was one pixel wide, light gray on dark gray background and consisted of a diagonal cross extending from corner to corner and four concentric circles at  $0.5$ ,  $5$ ,  $10$ , and  $15^\circ$  eccentricity. All subjects were experienced psychophysical observers and eye-tracker measurements indicated that the SD of fixation position during fMRI experiments was less than  $1/4^\circ$ . Subjects viewed stimuli displayed on a small translucent screen mounted on the head coil. The stimuli were projected using a LCD-projector placed in a shielded box at the foot of the scanner bed. This display system subtended  $\pm 16^\circ$  vertically and  $\pm 20^\circ$  horizontally. The display, calibrated by a PR-650 PhotoResearch Spectroradiometer, had a mean luminance of  $30 \text{ cd/m}^2$ .

### Data analysis

The functional data were analyzed using the Stanford VISTA-Tools and an improved version of the ATLAS-toolbox (Dougherty et al. 2003). The ATLAS tools estimate area boundaries by fitting a canonical scheme for V1–V3 simultaneously to retinotopic data for both the eccentricity and meridian sweeps (Fig. 1). It is semi-automated because the operator has to generate a starting scheme and control the results of the fit, which may terminate in local minima of the optimization. Repeated fits were therefore made with different starting points to confirm stable convergence to the V1–V3 region identified by eye at the first pass. The matrix inversion algorithms for this optimization are described in Fischer and Modersitzki (2004). This method estimates the boundaries between the visual areas and also the position of each isopolar or isoeccentricity line. This fit provided an objective method for identifying these key features, providing the basis for the analysis of this paper.

### Distance measurements

To specify the shape of cortical projection areas as accurately as possible, we estimated 3-dimensional distances along the cortical manifold using the Dijkstra algorithm in an overcomplete mesh of the boundary between white and gray matter. Measuring distances along a grid (in either 2 or 3 dimension) is subject to errors of the “city-block” type. The mesh was overcomplete in the sense of including all diagonals of the city-block connections because this reduces the city-block error significantly. We estimated the extent of this using a spherical model of the cortex and a Monte Carlo simulation. Irrespective of the radius of the sphere the error distribution was approximately normally distributed with a SD of only  $\pm 2.1\%$ . The method also results in a mean overestimation of distances by  $7.5\%$ , but we corrected this overestimation by dividing the measures by a factor of  $1.075$ , leaving only the residual error of  $\pm 2.1\%$  (see supplementary materials<sup>1</sup>). All distance measurements presented in this paper are measured using this method within the 3D manifold of the undistorted cortex.

## RESULTS

### Retinotopy

We performed retinotopic mapping on 8 subjects and analyzed areas V1 and V2 in the right hemispheres using the semi-automated atlas fitting procedure (Dougherty et al. 2003). Briefly this method fits a schematic model of the early visual areas (V1–V3) to the measured polar angle and eccentricity maps simultaneously (see METHODS). Its purpose is to determine

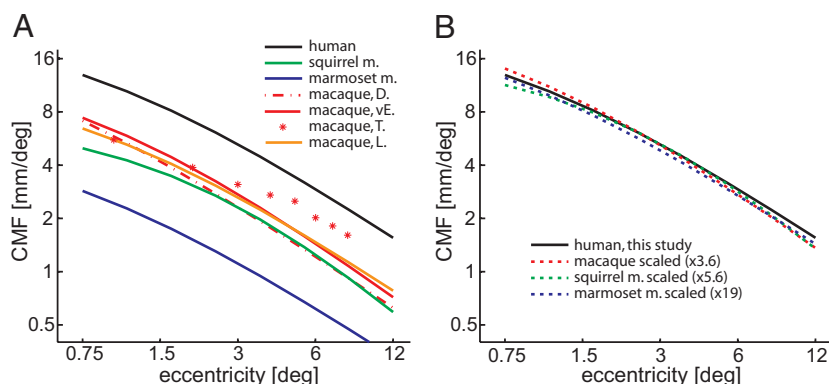


FIG. 3. *A*: comparison of linear cortical magnification factor (CMF) in V1 across primate species. The black line displays the V1 fit from this study, compared with results from van Essen et al. (1984), Dow et al. (1985), Le Vay et al. (1985), Tootell et al. (1988), Adams and Horton (2003), and Rosa and Tweedale (2000). *B*: for comparison, we scaled the results from the different monkey species so that they roughly match the human data in area. For macaque we used the data by Van Essen et al. (1984).

<sup>1</sup>The online version of this article contains supplemental data.

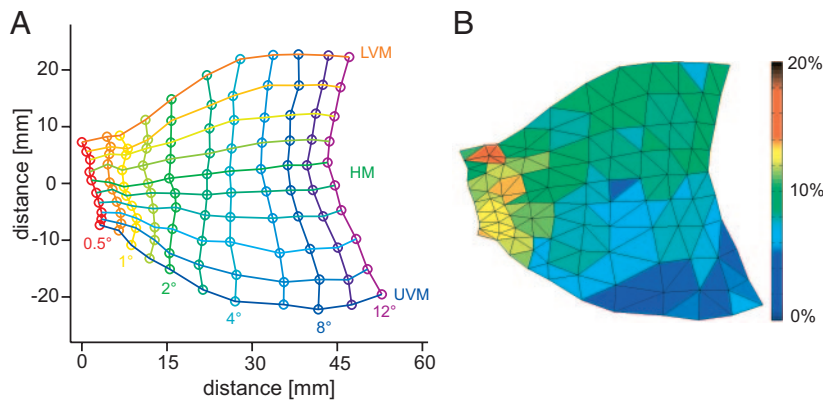


FIG. 4. *A*: 2-dimensional reconstruction of human V1 derived from our measurements. The colored numbers depict the isoeccentricity points, LVM, lower vertical meridian; HM, horizontal meridian; UVM, upper vertical meridian. *B*: map of local distortion of the reconstruction from the measured distances. The mean distortion is 9%, the highest distortion is 14%. This map depicts local error only, after the multi-dimensional scaling (MDS) optimizes the map for minimal error across all distances in the grid.

the borders between these early visual areas and to fit a smooth representation of both polar angle and eccentricity within these borders. We restricted our analysis to V1 and V2. For a reliable fit of V3, one would need a clear specification of the organization of its neighboring visual areas (V3A, V3B, hV4), which are still under dispute. Figure 1 shows two examples of our atlas fits.

#### Dependence of $M_A$ on eccentricity

The first parameter we measured was the classical eccentricity magnification function. Each subject's V1 was segmented into annular regions of  $\pm 15\%$  eccentricity at several eccentricities (e.g.,  $0.6\text{--}0.8^\circ$  for the  $0.7^\circ$  eccentricity and  $6.8\text{--}9.2^\circ$  for the  $8^\circ$  eccentricity). We then measured the size of each of these subregions to estimate the areal magnification  $M_A$  (in  $\text{mm}^2$  of cortex/ $\text{deg}^2$  of visual field) for these eccentricity ranges, averaged across the range of polar positions (from  $-\pi/2$  to  $\pi/2$  in radians or  $-90$  to  $+90$  in degrees). The square root of this number ( $M_{\sqrt{A}}$ ) is a linear measurement (the geometric mean of the magnification in the eccentricity and polar angle directions) and can be fitted by Eq. 1. It is these numbers ( $M_{\sqrt{A}}$ ) that we show in for V1 and V2 in Fig. 2.

It is interesting to note that V1 and V2 have a similar values for  $a$  ( $0.77$  vs.  $0.73$ ,  $t = 2.6$ ,  $\text{df}, 7$ , n.s.) but significantly different scaling parameters  $k$  ( $1.92$  vs.  $1.59$ ,  $t = 28.6$ ,  $\text{df}, 7$ ,  $P < 0.01$ ). As reported by Dougherty et al. (2003), there is considerable variability in the linear magnification function across subjects—particularly at eccentricities  $< 3^\circ$ . However, we find that these differences can be modeled as changes in the scaling parameter. After accounting for differences in the overall size of area V1, the form of the cortical magnification function is remarkably constant (Figs. 2*B* and S1).

The cortical magnification function has been described previously in several primate species and for macaque monkey by

several authors using different procedures and frameworks. In Fig. 3*A*, we plot several of these to allow a comparison between different species. For illustration, we multiplied the areal magnification functions  $M_A$  provided by these authors and multiplied them with the values depicted in Fig. 3*B*. We then took the square root of these numbers to obtain linear magnification ( $M_{\sqrt{A}}$ ). Moreover, the concept of inverse magnification has been found useful for characterizing the foveal singularity, such as Duncan and Boynton (2003), Levi et al. (1984), McKee and Nakayama (1984), Rovamo and Virsu (1979), Stensaas et al. (2001), and Tyler (2001). A plot of the average inverse magnification function for our V1 data (Fig. 2*C*), shows no significant deviation from a straight line with a negative intercept of  $-0.95$ .

#### Average map

To obtain an average 2D map of human V1, we identified the cortical locations for 10 meridians and 11 isoeccentricity rings (110 locations) in each subject's V1. The locations are specified as the voxels lying most closely within the cortical gray matter, defined for the zone 2 mm above the gray/white matter segmentation boundary (in the direction normal to this boundary). We then measured the distance between each pair of these 110 positions (6,050 distances per subject) along the 3D cortical manifold, resulting in a "distance grid" for each subject's cortical map. We averaged these distance grids to obtain an average distance grid, uncontaminated by any flattening distortions. This array constitutes the raw data for the specification of the shape of V1. This dataset is too large for publication in paper form, but we provide the data online because it represents an undistorted reference for the distances between the projections of these 110 visual field positions.

To fit our data to the available mapping models and present it in a digestible form for reference purposes, we projected the

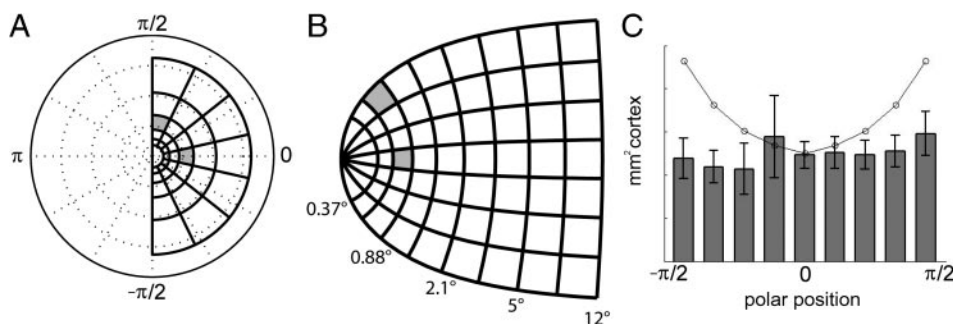


FIG. 5. Dependence of  $M_A$  on the polar position. *A*: central part of the visual field. *B*: conventional Schwartz complex-log model with  $a = 0.77^\circ$ . The gray quadrilaterals depict the projection from  $0.7$  to  $1.1^\circ$  eccentricity and  $25^\circ$  of polar angle, either at the horizontal or the vertical meridian. Note the significant difference in area with polar angle. *C*: measured area of the visual representation from  $0.5$  to  $1.5^\circ$  eccentricity at 9 different polar angles: the error bars represent SE across subjects. The curve depicts the area predicted by the Schwartz model.

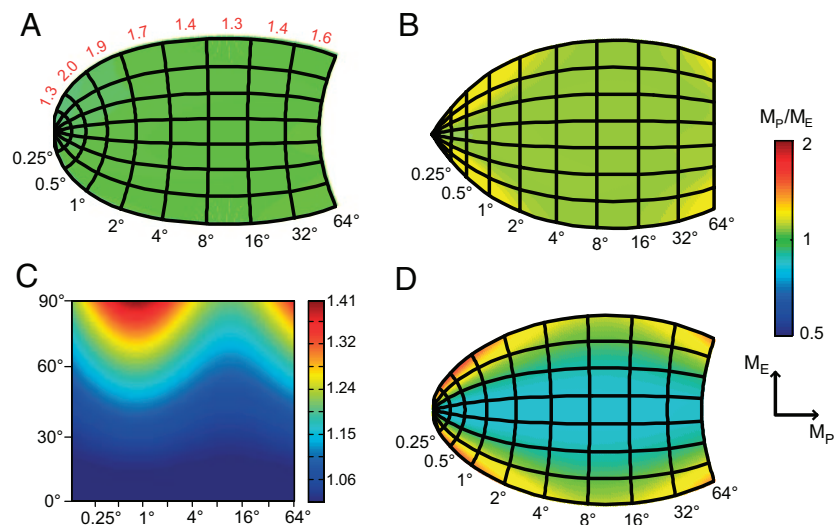


FIG. 6. The new models and the predicted local anisotropies. All models:  $a = 0.77$ ,  $b = 150$ ,  $k = 19.2$ , and no further parameters. *A*: Schwartz model predicts a complete local isotropy (that is  $M_P = M_E$ ) over the whole visual field, although at the cost of a severe meridional anisotropy. The red digits at the top signify the degree of anisotropy (in area ratio) between the horizontal and the vertical meridians, the coloration signifies *local* anisotropy. *B*: divisory model we suggest fixes the problem of meridional anisotropy, although at the cost of a small local anisotropy at the 4 corners of the projection. *C*: map of azimuthal shear for the parametric-2D-shear model. This figure shows only 1 quarter field,  $0^\circ$  being the horizontal meridian,  $90^\circ$  the vertical meridian. Note that this figure has a completely different colormap than *A*, *B*, and *D*. *D*: the parametric-2D-shear model depicted here has a balanced ratio where the average  $M_P/M_E = 1$ . This model predicts a complex pattern of local anisotropy, with  $M_P > M_E$  (bluish) at the horizontal meridian, whereas  $M_E > M_P$  (reddish) at the vertical meridian, as quantified in the color bar at far right.

3D data to a 2D surface. We reconstructed a 2D average V1 using a multi-dimensional scaling algorithm (metric MDS; Torgerson 1952). We flattened only once for the mean dataset rather than averaging several individually flattened cortices. The data for all the subjects were averaged in terms of the undistorted distances through the cortical manifold. This approach has several key advantages: the reconstruction is optimized to minimize the error within V1 only; the optimization is performed on a mean dataset with less noise than individual data; and the MDS algorithm gives a direct measurement of the amount of error introduced by the flattening. For our fits, the 2D reconstruction accounts for 95% of the variance in our data. This atlas for human V1 (shown in Fig. 4) provides a ready reference for the distance on the cortex between any two locations in the visual field.

#### Cortical area does not depend on polar position

Schwartz's complex-log models predict (as derived in the APPENDIX) that the area representing the vertical meridian is greater than the area representing the horizontal meridian (see Fig. 5, *A* and *B*). This meridional anisotropy reaches the theoretical maximum of a factor of 2 at  $a = 0.77^\circ$  eccentricity. We therefore made detailed measurements of this area in our

dataset. Specifically, we measured the area of cortex in V1 representing the central  $0.5$  to  $1.5^\circ$  of eccentricity at nine different polar angles (Fig. 5*C*). To avoid distortion, we performed all measurements in the 3D surface reconstruction of the cortical manifold (see METHODS). The average cortical area of the areal bins was  $52 \text{ mm}^2$ . There is no significant variation of areal magnification ( $M_A$ ) with polar position at the eccentricity where the complex-log model predicts a maximum variation.

#### Concept of equal-area

To clarify the amount of meridional anisotropy inherent in the Schwartz model, we estimated the ratio of the area representing a small square at the horizontal and the vertical meridians (see Fig. 6*A*, red digits, see also Fig. 5). The meridional anisotropy is 1 (or none) at the fovea, increasing up to a factor of 2 (in area) at  $0.77^\circ$  (at  $E = a$ ), then decreasing again toward the periphery. In peripheral regions, the predicted anisotropy increases again (as  $E$  approaches  $b$ ). In short, the Schwartz model predicts that there is up to twice as much visual cortex associated with the vertical meridian than the horizontal meridian and does so in a critical part of the visual field: the fovea.

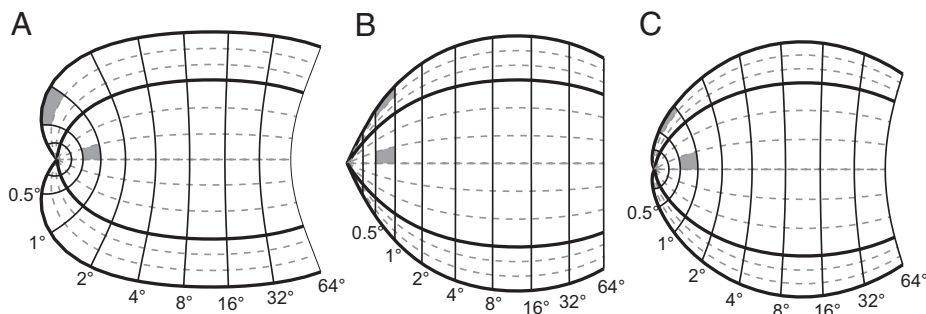


FIG. 7. Modification of the Wedge-Dipole model. *A*: the model as proposed by Balasubramanian et al. (2002) with  $a = 0.9$  and  $b = 170$ ,  $a_1 = 0.95$   $a_2 = 0.5$ . The gray areas represent the same part of the visual field in V1 and V2 at the eccentricity where  $E = a$ . The model predicts a dramatically larger representation of the central part of the visual field in V2 than in V1 (270%). *B* and *C*: same parameters but using the divisory model (*B*) and using the parametric-2D-shear model (*C*). The latter 2 models predict not a larger but a smaller representation in V2 than in V1 (55%, when using the same parameters as in Balasubramanian et al. (2002); we suggest a larger value for  $\alpha_2$  resulting 80% of the area); however, all 3 models suggest that the representation in V2 is strongly elongated with respect to V1.

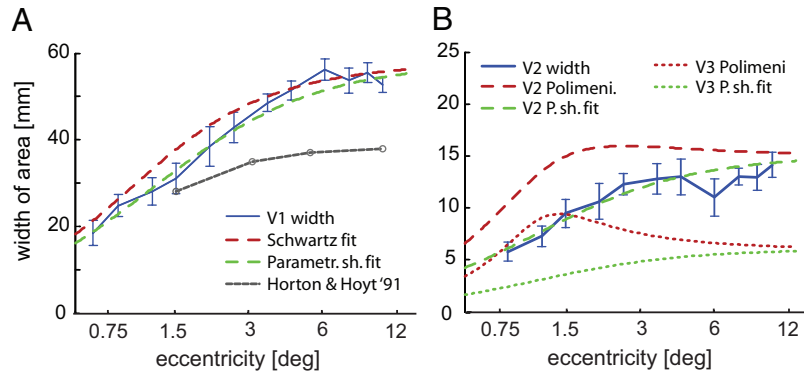


FIG. 8. A: width of V1 vs. eccentricity. The blue curve shows the data averaged across 8 right hemispheres error bars indicate the SE. The gray curve depicts widths measured from the sketch of Horton and Hoyt (1991a, Fig. 8), which is clearly narrower than our data. The red curve is the prediction of the Schwartz model, based solely on the parameters  $a$  (0.77) and  $k$  (19.2) from our fit of  $M_{\sqrt{x}}$ . The Schwartz model is an impressive approximation of the observed retino-cortical mapping widths. However, the prediction is too wide between 0.5 and 3° eccentricity, a symptom of the meridional anisotropy that we report in Fig. 5. We plot the prediction from the parametric-2D-shear model as the dashed green line. B: width of V2 vs. eccentricity. The blue curve shows our V2 data averaged across 8 subjects. The red curves show the prediction from the Schwartz and Balasubramanian model (2002), the dashed green curve shows the prediction from the parametric-2D-shear model (dashed lines, V2; dotted line, V3; although we did not measure V3 data). The prediction of the Schwartz model significantly overestimates the width at small eccentricities, whereas our model corrects for this. Note that we used the parameters suggested by Balasubramanian et al. (2002) throughout.

We did not observe the meridional anisotropy near  $a$  as predicted by the complex-log model in our fMRI data (Fig. 5C). Squirrel monkey data from Adams and Horton (2003) are consistent with these observations. We therefore suggest a new model that would preserve meridional isotropy of the area ( $M_A$ ) at the expense of a small degree of local anisotropy (linear, ratio of  $M_E/M_P$ ).

In principle, there are several ways to achieve equal-area meridional mapping. A mathematically simple approach is to ensure that the imaginary part (azimuth or polar position) of the complex-log transform stays small. In practice, our suggestion is to first divide the polar position value by a large number (the larger the better, in practice 5 is sufficient) and subsequently multiply the real part of  $w(P,E)$  by the same value (to form the divisory model).

$$w(E,P) = k * \{ \text{real}[\log(E * e^{i^*P/\eta} + a)] + \text{imag}[\log(E * e^{i^*P/\eta} + a)] * \eta \} \quad (3)$$

in the limits as  $\eta \rightarrow \infty$  For  $\eta = \infty$ , the derivative of this function is Eq. 1. Although Eq. 3 solves the meridional anisotropy, it does so at the expense of a strong compression of the local angles in the central fovea (Fig. 6B). To avoid this compression, we introduce a second method that takes an iterative approach to solving the problem of meridional anisotropy by a parametric shear of the polar angle magnification (parametric-2D-shear model). This model calculates the projected area for a given eccentricity and various polar angle ranges starting from the horizontal meridian. The increase of projected area further away from the horizontal meridian is then corrected iteratively by the application of successive local rotational shears in the polar direction. This operation results in the 2D shear map presented in Fig. 6C resulting in an equal-area model (Fig. 6D), note that the amount of shear varies with eccentricity and polar position. This model has near-zero meridional anisotropy (<0.1% after 10 min of iteration) at the cost of introducing a local anisotropy (indicated by the coloration in Fig. 6D).

Because this iteration process is time consuming, we approximated the numerical fit with a 2D shear function that provides the same map within 0.3% of the iterative result.

Accordingly we suggest the mapping function

$$w(E,P) = k * \log(E * e^{i^*P * f_a(E,P)} + a), \quad (4)$$

where  $f_a(E,P)$  is a shear function that can be either determined iteratively or using the simple closed form approximation

$$f_a(E,P) = \text{sech}(P)^{\text{sech}(\log(E/a) * S_1) * S_2}, \quad (5)$$

where  $S_1$  (=0.76) and  $S_2$  (=0.18) are not free parameters, but optimized to provide an optimal approximation to the shear function  $f_a(E,P)$  resulting in an equal area model. This double-sech approximation provides a near optimal fit over a wide range of  $a$  or  $b$ . The 2D shear function was chosen by inspecting the iteratively determined shear function. The fact that the functions that combine to describe the shear are both hyperbolic secants may be coincidence. However, the  $\text{sech}(P) - \text{sech}(\log(E))$  combination of Eq. 5 gave a particularly accurate approximation to the iterative determined shear. A third parameter  $gISh$  can be used to apply a global shear, analogous to the rotational shear  $\alpha_1$  suggested by Balasubramanian et al. (2002), but may not be necessary. We fitted these

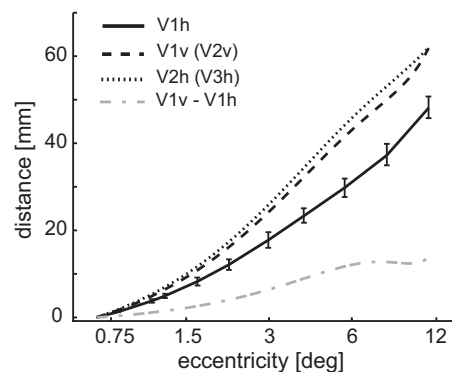


FIG. 9. The length of isopolar lines. The solid black line shows the cumulative length for the horizontal meridian in V1 averaged across 8 subjects; error bars depict SE. The dashed black line shows the vertical meridian of V1 (i.e., the V1/V2 border). The dotted black line is for the horizontal meridian at the V2/V3 border. The dash-dotted gray curve shows the length difference for the horizontal vs. vertical meridians in V1.

three models to our V1 data and found that both the divisory and the parametric-2D-shear model describe our data better than the models proposed by Schwartz and its variations proposed by Balasubramanian et al. (2002). (We provide additional descriptions, fits and errors, including Matlab code demonstrating the models, in supplementary materials).

In 2002, the Schwartz group proposed an intriguing extension of their model, the wedge-dipole model (Balasubramanian et al. 2002). This model presents a simple way to integrate V1–V3 into one single mapping function, potentially providing the possibility of predicting the detailed properties of these visual areas, by introducing a single polar shear/scaling parameter  $\alpha_1$ ,  $\alpha_2$ ,  $\alpha_3$  for each retinotopic area. Unfortunately, the wedge-dipole model suffers even more from the meridional anisotropy flaw of the original Schwartz model (Fig. 7A). Our equal-area models fix this problem not only for V1 but also for V2 and V3, making the approach suggested by Balasubramanian et al. (2002) feasible. The correction is shown for the divisory and the parametric-2D-shear models in Fig. 7, B and C.

### Widths of V1 and V2

The widths of area V1 and its neighboring maps (V2, V3) are important properties of the visual cortex mapping. However, these widths have never been measured systematically. All current models of V1 assume that at the representation of the center of the visual field, the width of V1 is 0. The width of V1 then increases with eccentricity until it reaches a maximum at  $\sim 12$ – $16^\circ$ . It then decreases again at the peripheral end of the representation (see V1 diagram from Horton and Hoyt 1991a; their Fig. 3). Imaging data for human visual areas are usually presented as flatmaps, computationally unfolded and flattened approximations of the cortical surface (DeYoe et al. 1996; Press et al. 2001; Sereno et al. 1995; Tootell et al. 1996; Van Essen et al. 2001). These illustrations are useful for visualization purposes, but the computational flattening distorts the true shape of V1. We therefore measured the widths of V1 and V2 along isoeccentricity lines through the 3D cortical manifold. Our measurements show that the widths of both areas increases steadily from  $0.5$  to  $8^\circ$  eccentricity, a key property of human V1 and V2 that has not been previously quantified. The sketch of human V1 provided by Horton and Hoyt (1991a); for example, suggests that human V1 reaches its maximum width as early as  $2.5^\circ$  eccentricity (Fig. 8).

### Lengths of the meridians

All the retino-cortical projection functions described so far share one effect of polar position: the representation of the vertical meridian is longer than that of the horizontal meridian. If the cortical manifold can be flattened without distortion, it follows that the true lengths for the meridians, as measured on the 3D cortical sheet, must differ as well. To test if this particular effect of polar position is present in our data, we measured the lengths of lines of constant polar angle within cortex. For each line, we plotted eccentricity in visual space against cortical distance. Crucially, these measurements were made in the undistorted 3D cortical manifold and they provide a critical test of whether V1 can be described with 2D models.

We found that in V1 the average vertical meridian representation ( $n = 8$ ) is longer than the average horizontal meridian

representation by a factor of  $1.26 \pm 0.06$  over the range  $0.5$ – $12^\circ$  eccentricity (Fig. 9) very close to the predicted factor of 1.27. The lengths of these isopolar meridians increase gradually with polar angle, and there was no difference between the upper and lower visual fields (see supplementary material). These results match the predictions from our models (see supplementary materials). This match between the measured lengths and the planar model with no intrinsic curvature suggests that there is little intrinsic curvature in V1. The consequence of the difference in length between the two meridian lines is that  $M_P$  depends on polar position: it is larger for the vertical meridian than for the horizontal meridian. Because  $M_A$  is independent of  $P$  (Fig. 5),  $M_E$  must vary with  $P$  as well. And because  $M_A = M_E * M_P$ , the local anisotropy ( $M_E/M_P$ ) must vary with polar position as well.

We now consider the length of the next horizontal meridian representation, the V2/V3 border. It is interesting that the V2/V3 border length is very similar to that of the V1/V2 border as well as the intermediate, i.e., oblique, isopolar meridian in V2 (not shown). This means that  $M_P$  at the V2/V3 horizontal meridian is roughly the same as on the V1/V2 border but is significantly different from  $M_P$  at the horizontal meridian in V1 despite the fact that they represent the same part of the visual field. Because  $M_P$  is larger in V2 than in V1, whereas V2 has a smaller areal magnification than V1, it follows that  $M_E$  in V2 has to be much smaller than in V1. In other words, there is large local anisotropy in V2 with  $M_P$  being about twice the value of  $M_E$  on average.

### DISCUSSION

We have presented a new dataset that allows us to test different models of the way that visual space is mapped to visual cortex. As is well known, the dominant principle in these mappings is a compression of the visual field representation with eccentricity. This compression is approximately logarithmic, with a small offset to avoid an infinite magnification in the center of the visual field (Fig. 2C). Areas V1 and V2 both contain complete maps of visual space and because they share borders; their shapes are highly constrained especially in and around the foveal confluence.

These constraints set up competing requirements among global isotropy, local isotropy, and local conformality of the V1 map and of the two segments of the V2 map lying adjacent to it. In principle, these requirements could all be satisfied if the maps had appropriate intrinsic curvature, but violations of one or other of these principles are necessary if the maps are intrinsically flat or if the curvature is constrained by other factors. Our detailed measurements assess both the intrinsic curvature of the mappings and the particular solution that has evolved in the human brain among the competing mapping principles.

We first consider the foveal measurements in the present study and how they constrain the layout of the foveal confluence. We then discuss the assumptions and implications of the three-dimensional shape of visual cortex, and why we think that flat models for V1 are useful. Finally, we discuss inter-subject variability and show that it consists of predominantly a scaling factor and with little variation in the other mapping parameters.

### Measuring the fovea

One of the most important contributions of this paper is to provide detailed data down to  $0.5^\circ$  of eccentricity. Retinotopic mapping in the fovea is technically challenging, and consequently data from this region are not usually analyzed in studies of human cortical magnification. One of confounding factors for foveal measurements is the occurrence of spontaneous eye movements. Assuming that subjects fixated most of the time and that eye movements are random, sufficient averaging should reveal the mapping up to the centermost part of the visual field with gradually increasing noise toward the center of the fovea. Although all subjects are instructed to maintain fixation at the center of the fixation cross, some eye movements are inevitable. However, the use of an invariant fixation grid while viewing the cycling retinotopic stimulus provided substantial improvement in the fixation accuracy during the scans and repeated averaging reduces the effects of momentary eye movements. In separate experiments, we made high-precision measurements of our subjects' ability to fixate by presenting the retinotopy stimuli while simultaneously imaging the fovea using a Rodenstock scanning laser ophthalmoscope. On average, our subjects fixated during retinotopic stimulation with an SD of only 11 arc min. Our measurements of subject fixation in the MR scanner are consistent with this value although our MR eyetracker can only measure with a precision of 20 min of arc.

Another problem with measuring at the foveal representation is the limited spatial resolution of fMRI. Based on the analysis of this paper, the average human foveal projection ( $0-0.5^\circ$  of eccentricity) of V1 covers an area of  $142 \text{ mm}^2$  ( $\sim 14$  voxels) and is  $\sim 17 \text{ mm}$  ( $\sim 5$  voxels) wide at  $0.5^\circ$  while being only  $9 \text{ mm}$  ( $\sim 3$  voxels) wide at  $0.25^\circ$  eccentricity. This calculation illustrates how difficult it would be to measure the widths of V1 and V2 at  $0.25^\circ$  eccentricity, where each half of V2 would be only  $\sim 4 \text{ mm}$  wide (i.e., the V2/V3 border is little more than a voxel away from the V1/V2 border). To image the last  $0.5^\circ$  of the fovea, one would therefore need higher-resolution scans. We estimate that using  $1.5^3 \text{ mm}$  voxels would allow substantially better detail, allowing one to map down to  $0.2^\circ$  eccentricity.

### Layout of the foveal confluence

The maps of the early visual areas V1, V2 (dorsal and ventral), and V3 (dorsal and ventral) converge toward a "foveal confluence" near the occipital pole in human brains (Brewer et al. 2005; Dougherty et al. 2003; Press et al. 2001; Sereno et al. 1995; Tootell et al. 1996). Unfortunately, the layout of early visual areas at the very center of the fovea remains unclear. All current theoretical models based on the Balasubramanian wedge-dipole layout propose that V1, the two halves of V2, and even the two halves of V3 meet at a single point. Current anatomical reviews in monkeys, however (Rosa and Tweedale 2005 for marmoset; Gattass et al. 2005 for cebus and macaque), suggest that V2 does not come down to a point but rather forms a strip with significant width. Our measurements indicate that if V2 forms a strip at the fovea, at least in humans this strip is not more than  $7 \text{ mm}$  wide at  $0.5^\circ$  (see Fig. 8B). Gattass et al. (2005) on the other hand suggests a rather wide strip of V2 from  $0 \leq 2^\circ$  eccentricity, even proposing a larger

representation of foveal V2 than foveal V1. This is in clear disagreement with the width data we present here (see Fig. 8; V2 is narrower than V1 at every eccentricity). The results of Rosa and Tweedale (2002) on the other hand indicate that this strip narrows down  $< 1 \text{ mm}$  in the tiny brain of the marmoset monkey.

### Flatness of human V1 or the "rugby ball" concept

All published models of the properties of human V1 would be invalid if human V1 contained significant intrinsic curvature. One could imagine that human V1 was intrinsically ellipsoidal, having the 3D shape of the surface a rugby ball (or a part of it), where the poles represent the fovea and the far periphery. Each seam on the rugby ball would represent a different polar angle, and each one could thus have precisely the same geometry, allowing a log-polar projection function with ideal properties: local and global isotropy as well as conformality of the angular mappings. Any 2D projection of this ideal mapping would, however, introduce systematic distortion ruining these perfect properties. A similar argument was presented by Rovamo and Virsu (1984), arguing that macaque operculum is not flat. Although we know that human V1 is a convoluted manifold in 3D space, it appears that the V1 geometry is intrinsically flat and only folded within the calcarine sulcus (see following paragraphs). Human V1 may, thus, be more folded but appears to be flatter than for example squirrel monkey V1, which incorporates substantial intrinsic curvature (D. L. Adams, personal communication). Kaplow and Schwartz (1986) investigated the flatness of macaque V1 and came to the conclusion that the error due to flattening is small (5%) and therefore intrinsic curvature is negligible. However, the fact that the average distortion is small means neither that it is not systematic nor that is small in every location.

The strongest argument for human V1 being intrinsically flat is the increasing length of the isopolar lines with polar angle from the horizontal meridian (see Fig. 9, and supplementary materials). While a rugby-ball-shaped V1 would imply that the lines should have equal length, any flat V1 model consistent with our data would predict that these lengths increase with polar angle. Tootell et al. (1988) reported such a result in macaque. However, these measurements were made in a flattened macaque cortex, and the difference might possibly have been due to some flattening distortion. Here, we measure the same effect directly in the folded and unflattened cortex, providing strong evidence that human V1 is at least not a perfectly symmetric rugby ball. Further, the strength and layout of the anisotropy matches the predictions from our flat model (supplementary Fig. 3), suggesting that V1 is indeed intrinsically flat.

For V2 the situation is different, however. Although the models we propose in Fig. 7 assume that both V2 and V1 lie within a homogeneous flat plane, this may not be the case. To our knowledge, the flatness of V2 has not been investigated so far. The equal-area maps of Fig. 7B and C, illustrate that an equal-area planar map of V2 must violate conformality. Maintaining conformality in a flat V2 would require a huge degree of meridional anisotropy (see Figs. 7A and 8B, red lines). Both problems could be solved if the V2 mapping were intrinsically ellipsoidal (the rugby-ball model). In this context, it is interesting to note that—in contrast to V1—all measured V2-

meridian representations from horizontal through vertical, have the same length within the precision of our measurement. This suggests that V2 is probably best described with the rugby-ball model rather than the intrinsically flat and only folded variants of the Balasubramanian model. We do not have sufficient material to test this hypothesis further, but we present and illustrate it in supplementary materials.

#### *Reconstructed average map of human V1*

Because we did not find systematic curvature in V1, we reconstructed a 2D reconstruction of human V1 in Fig. 4A. This map allows a ready reference for the average distance between the representations of visual field locations on human primary visual cortex. An interesting feature of this reconstruction is that the isoeccentricity lines beyond 8° appear convex, with their representation around the horizontal meridian closer to the fovea than the ends of the isoeccentricity representations. This is an interesting feature that is strongly present in the data from Tootell et al. (1988) where it is clearly evident as early as 3° of eccentricity. Although the dipole model proposed by Schwartz (1983) predicts such convex isoeccentricity lines, the strength and the onset at small eccentricities would suggest a very small value for  $b$ . A very small  $b$ , however, would put several other constraints on the model (see supplementary materials).

The map of local deviation of the reconstruction (Fig. 4B) with the originally measured grid shows that there is more local error in the perifoveal part of the reconstruction and more error in the ventral half than in the dorsal half. We did not find any other significant difference between the ventral and the dorsal half of V1. The higher error in the foveal part of the reconstruction could be explained by the fact that smaller distances are more difficult to measure (see supplementary materials).

#### *Intersubject variability*

Dougherty et al. (2003) investigated the representation of the visual field in V1–V3 of six human subjects using a similar methodology. The Dougherty et al. study illustrated the high degree of intersubject variability in V1 area (up 2.4 times; see also Stensaas et al. 1974). We confirm these results: the largest V1 in our sample has 2.3 times the area of the smallest. However, as we illustrate, these extreme cases basically differ in overall size and have no significant difference in the shape of their V1s (see supplementary materials). This invariance is consistent with the finding by Tootell et al. (1988) that magnification correlates with the size of striate cortex.

It could be argued that due to the substantial variation between different subjects' V1s, there is little point in making a detailed average. If one is not in a position to measure the V1 morphometry for individual subjects, however, a good average is certainly the best estimate of its parameters. This is also true if we wish to relate cortical magnification to psychophysical data averaged across subjects. Besides, it is worth noting that a maximum variation of 2.3 in area reflects a factor of only 1.5 in linear size and that the SD of our  $k$  parameter is only  $\pm 15\%$ .

#### *Is visual cortex conformal?*

One of the central questions to distinguish the different variants of models proposed here is the degree to which they

exhibit conformality of the angular mapping. The original Schwartz model is perfectly conformal for V1, such that right angles in the visual field project to right angles on cortex, for example. However, subsequent refinements to this model introduce a shear in the polar angle direction (Balasubramanian et al. 2002), and, as the authors note, this eliminates conformality. Unfortunately there are no good estimates as to how conformal the organization of visual cortex is, and even the benefits of a conformal visual cortex are unclear. This issue is even less clear when considering V2 and V3. In the fovea, there is theoretically space only for a conformal V1 and V2 (leaving no room for V3), but this conformality can be achieved only at the cost of a strong meridional anisotropy between the horizontal and vertical meridian representations. That is, conformality would produce a small horizontal meridian and large vertical meridian representations in V1, with the opposite arrangement in V2). However, this does not match our data (Figs. 9 and S3).

#### *Different forms of magnification and anisotropy*

Our results agree with current estimates of cortical magnification in humans (Dougherty et al. 2003; Levi et al. 1984; Slotnick et al. 2001), but cortical magnification must be considered as a 2D property of visual cortex, depending on both eccentricity and polar position. When investigating cortical magnification, for example using psychophysical methods, it is essential to be clear about what kind of magnification one is investigating (linear or areal), and it is also important to map it in both dimensions of the visual field. The models that we have developed (Figs. 6 and 7) enforce equal-area magnification within each eccentricity range. This uniformity comes at the cost of a systematic pattern of *local* anisotropy. In particular, we predict large differences in local anisotropy on the horizontal and the vertical meridian representations at  $\sim 0.77^\circ$  eccentricity.

Most psychophysical studies relating performance to (presumed) cortical area have used relatively eccentric stimuli. We suggest that investigation of such properties at the critical eccentricities  $< 1^\circ$  would allow a test of the predictions we make here, possibly improving the fit of the parameters  $a$ ,  $b$ , and  $k$ . Such studies could also evaluate the intersubject variability of the parafoveal mapping in the manner used by Duncan and Boynton (2003) for analyzing mapping functions beyond  $1.5^\circ$  eccentricity.

#### *Ocular dominance columns and anisotropy*

One of the most prominent anatomical features of human and macaque V1 are the ocular dominance columns (Horton and Hedley-Whyte 1984; LeVay et al. 1975). These and other substructures of visual maps are not part of any current retino-cortical projection model. There is strong evidence that each of these substructures contain continuous representations of most parts of the visual fields, and that these maps are interdigitated (Blasdel and Fitzpatrick 1984; Shipp and Zeki 2002; Tootell et al. 1988) into the overall map of a given area. However, in V1 these interdigitated maps are shown in the monocular input layers (Blasdel and Fitzpatrick 1984; Tootell et al. 1988) and may not extend throughout the binocular layers.

In V2 Shipp and Zeki (2002) have termed the organization of these submaps a "ratchet model" and demonstrated that the

mean of each of the  $\sim 1$  mm wide stripes follows the continuous macro map, a concept that could easily be integrated into the current models. With the current resolution of fMRI being 3 mm, however, these micro deviations are invisible. Tootell et al. (1988) found local anisotropy in macaque V1 but no overrepresentation (in area, as estimated by width) of the vertical versus the horizontal meridian. They suggest that the pattern of local anisotropy is associated with the pattern of ocular dominance columns. To be precise, they suggest a higher magnification perpendicular to the ocular dominance columns than along them. We would like to point out that this is precisely the same pattern suggested by our parametric-2D-shear model. Based on this model, we would suggest a magnification of roughly 1.4:1 (perpendicular/parallel) across pairs of ocular dominance columns (or in layer 2/3 and 6 or in the macro map), implying a ratio of 0.7:1 within one ocular dominance column (or within the micro map).

The pattern of local anisotropy suggested by our model matches the pattern observed in several monkey species (Gattass et al. 1987 for cebus monkey; Tootell et al. 1988 for macaque monkey; Fritsches and Rosa 1996 for marmoset monkey, Adams and Horton 2003 for squirrel monkey). In short: sectors along the horizontal meridian are compressed along eccentricity axis, whereas sectors along the vertical meridians are elongated (see Fig. 6D).

For V2, we suggest (and measure) an overall anisotropy of 2:1, that is V2 is elongated along the eccentricity direction or parallel to the stripe structure. Assuming that the complete eccentricity range is represented in each of the three stripe types, this would result in a local anisotropy of  $\sim 0.66:1$  within a stripe.

### Conclusions

Cortical magnification is a 2D property of visual cortex, depending on both eccentricity and polar position. It can be described in terms of either linear magnification (in various directions) or areal magnification. When investigating cortical magnification, it is important to express the magnification function for both axes of the maps in terms of both the local and global anisotropies of the mapping. We provide high-density mapping data from many subjects over an extended range of eccentricities and derive an accurate mapping formalism (Eq. 5) that accounts for the cortical morphometry of the first-tier retinotopic areas within a geometric error of 0.3%.

### APPENDIX

#### Cortical magnification in two dimensions

The concept of cortical magnification was introduced by Talbot and Marshall (1941) and described as a function by Daniel and Whitteridge (1961), who defined it as the displacement of two cells in millimeters on the cortex divided by the displacement of their receptive field centers in degrees (in units of  $\text{mm}/^\circ$ ). This is a 1-dimensional measurement and accordingly magnification is often specified as:

$$M(E) = \frac{k}{E + a}, \quad (A1)$$

where  $E$  is the eccentricity of the receptive field (in  $^\circ$ ) and  $k$  (in mm) and  $a$  (in  $^\circ$ ) are free parameters. Note that, in this formulation, the magnification is assumed to be independent of azimuthal position in

the map (which we will call "polar angle,"  $P$ ). If this assumption is relaxed, then  $M$  becomes a function of both  $E$  and  $P$ , requiring the definition of two magnification directions,  $M_E$  and  $M_P$  that combine into a full 2D function. The assumption that the angular position has no effect on the magnification is based on two observations (Daniel and Whitteridge 1961).

First, the cortical magnification is the same in both the angular and radial directions ( $M_P = M_E$ ). For clarity, we will call this local isotropy (or anisotropy, where violated). However, it is important to note that later studies indicate that V1 may show only approximate local isotropy. For example, Adams and Horton (2003) find a pattern of systematic local anisotropy in V1 of the squirrel monkey.

Second, the cortical magnification for a given eccentricity is the same at different angular positions. This means that the cortical magnification changes with  $E$ , but not with  $P$ , and is therefore identical along the horizontal and the vertical meridians for a given eccentricity. We will call this property meridional isotropy (but see Van Essen et al. 1984 for a report of meridional anisotropy in macaque monkey).

It is important not to confuse these two properties of the magnification parameters. The degree of local (an)isotropy says little about any meridional difference between the horizontal and the vertical meridians (or intermediate meridians), and the degree of meridional (an)isotropy says nothing about the local ratio between  $M_P$  and  $M_E$  at a given point of the visual field. In this paper, we show that V1 exhibits local anisotropy, but a reasonable degree of meridional isotropy is found for the areal magnification  $M_A$ .

Areal magnification (Myerson et al. 1977; Tusa et al. 1978) is a 2D metric: the area of cortex per area of visual field [ $M_A(E,P)$ , in  $\text{mm}^2/\text{deg}^2$ ], where  $(P,E)$  are the coordinates of the visual field. Areal and linear magnifications are closely related. Specifically,

$$M_A = M_E * M_P. \quad (A2)$$

If  $M_E$  and  $M_P$  are the same (isotropy), they are also the equal to  $\sqrt{M_A}$ .

In short, areal magnification, as well as the linear magnifications in any direction, are 2D functions of both visual field dimensions. The analysis of any of these functions in terms of one of its dimensions has to be parameterized by the other, orthogonal, dimension. In particular, any magnification as a function of eccentricity may be specified separately for the horizontal meridian by  $M(E,0)$  and at the vertical meridian by  $M(E,p/2)$ , respectively (see Fig. 6).

Schwartz (1994) pointed out that the linear magnification is a partial derivative of the overall retino-cortical projection function  $w(E,P)$ . To be precise, there are three interesting derivatives of this function: we can consider the partial derivative with respect to eccentricity which yields the conventional linear eccentricity magnification function, along lines of constant angular position:

$$M_P = \frac{\partial w}{\partial E}. \quad (A3)$$

We could also consider the partial derivative with respect to polar angle, giving the polar magnification function along lines of constant eccentricity:

$$M_E = \frac{\partial w}{\partial P}. \quad (A4)$$

Finally, we can compute an areal magnification function that takes account of both of these quantities:

$$M_A = \frac{\partial w}{\partial E} * \frac{\partial w}{\partial P}. \quad (A5)$$

Different forms of magnification ( $M_P$ ,  $M_E$ ,  $M_A$ ) as well as the retino-cortical mapping function are frequently estimated in both physiological and psychophysical experiments and to interpret them clearly it is important not to confuse the definitions.

### Retino-cortical mapping function

It is clear that the various forms of the cortical magnification function depend on the form of the retino-cortical mapping function  $w(E, P)$ . Schwartz (1977) proposed that this function can be approximated by:

$$w(E, P) = k * \log(E * e^{i^j} + a), \quad (A6)$$

and noted that the derivative of this function is “in the order of”

$$w' = \frac{k}{E + a} \quad (\text{see Eq. A1}). \quad (A7)$$

In fact, we point out that the exact derivative of the Schwartz function (Eq. A6) is:

$$M_P = \frac{\partial w}{\partial E} = k * \frac{e^{i^j P}}{E * e^{i^j P} + a}. \quad (A8a)$$

This derivative is a function of  $P$  and consequently is not independent of  $P$ . When  $P = 0$  (at the horizontal meridian) or when  $E$  is much greater or much less than the free parameter  $a$ , the expression reduces to Eq. A7, but for eccentricities close to  $a$ , the effect of  $P$  is significant. At the eccentricity  $E = a$ , it becomes

$$\frac{\partial w}{\partial E}(P) = k * \frac{e^{i^j P}}{a * (e^{i^j P} + 1)}. \quad (A8b)$$

The eccentricity magnification function is thus strongly dependant on  $P$  and changes by a factor of  $\sqrt{2}$  between the horizontal and vertical meridians. In short, the Schwartz complex-log projection entails a strong dependence on polar position  $P$  in the neighborhood of the eccentricity of parameter  $a$ .

Estimates of the magnification function based on mapping theory (Schwartz 1977, 1994), on anatomical measurements (Horton and Hoyt 1991a), or on psychophysical estimates (Levi et al. 1984; Yap et al. 1987) suggest a value of  $\sim 0.75^\circ$  for  $a$ . [Dow et al. (1981, 1985) give a lower value, but their data were reinterpreted by Levi et al. (1984) to be compatible with the  $0.75^\circ$  value]. The Schwartz model therefore predicts the strongest global anisotropy around the perifoveal eccentricity of  $0.75^\circ$ .

The original Schwartz model only describes the singularity at the foveal portion of the projection function. In a figure caption, Schwartz (1983) extended the complex-log transform to a dipole model to account for the peripheral mapping behavior. This model (Fig. 6A) introduces a third parameter  $b$ , creating a second singularity in the periphery:

$$w(E, P) = k * \log[(E * e^{i^j P} + a)/(E * e^{i^j P} + b)], \quad (A9)$$

or, if simplified to consider only the horizontal meridian by setting  $P = 0$ :

$$w(E) = k * \log[(E + a)/(E + b)]. \quad (A10)$$

Under this assumption, the dipole model generates a more complicated expression for the magnification function:

$$w'(E) = k * \frac{b - a}{(E + a)(E + b)}. \quad (A11)$$

It is important to note that this expression for the V1 map introduces curvature into the magnification function that corresponds to the third-order term introduced by Rovamo and Virsu (1979) into their power series expression for their magnification function. The dipole model thus provides a simpler approach to the same concept. However, just as estimating the parameter  $a$  requires precise measurements in the fovea, estimating the parameter  $b$  requires good peripheral data. This dipole model has received considerably less attention than the original model and there are no good estimates of  $b$ . Magnification

data including peripheral data are therefore usually fit to a power function (Adams and Horton 2003; van Essen et al. 1984) rather than to Eq. A11. Those studies that have attempted to estimate it give a value for  $b$  between  $90$  and  $180^\circ$  (Balasubramanian et al. 2002).

In conclusion, there has been no previous publication of the exact form of the 2D magnification function implied by the complex-log transform, which is widely regarded as an adequate characterization of the cortical mapping function. Our analysis reveals that the exact form of this is meridionally anisotropic and that no mapping onto a planar metric can simultaneously preserve the meridional isotropy, local isotropy, and conformality of the resultant map.

### REFERENCES

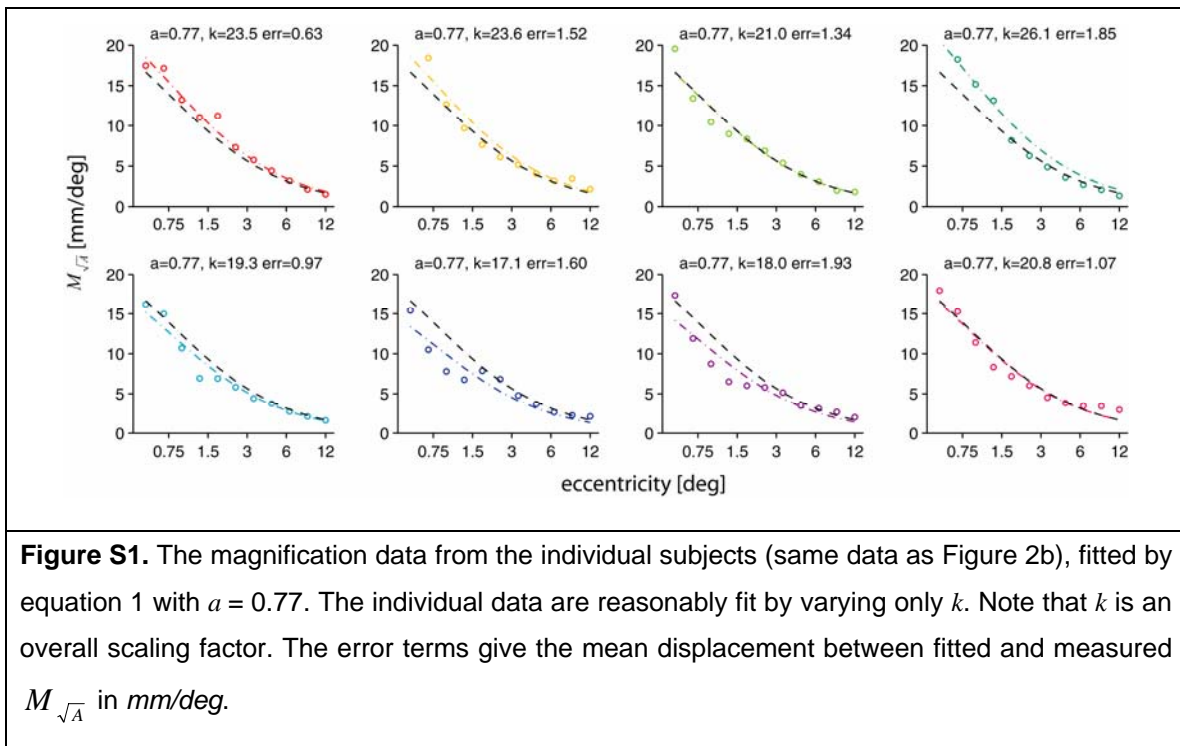
- Adams DL, Horton JC.** A precise retinotopic map of primate striate cortex generated from the representation of angioscotomas. *J Neurosci* 23: 3771–3789, 2003.
- Balasubramanian M, Polimeni JR, Schwartz EL.** The V1–V2–V3 complex: quasiconformal dipole maps in primate striate and extra-striate cortex. *Neural Networks* 15: 1157–1163, 2002.
- Battista J, Kalloniatis M, Metha A.** Visual function: the problem with eccentricity. *Clin Exp Optom* 88: 313–321, 2005.
- Blasdel GG, Fitzpatrick D.** Physiological organization of layer 4 in macaque striate cortex. *J Neurosci* 4: 880–895, 1984.
- Brainard DH.** The psychophysics toolbox. *Spat Vis* 10: 433–436, 1997.
- Brewer AA, Liu J, Wade AR, Wandell BA.** Visual field maps and stimulus selectivity in human ventral occipital cortex. *Nat Neurosci* 8: 1102–1109, 2005.
- Buchanan-Smith HM, Heeley DW.** Anisotropic axes in orientation perception are not retinotopically mapped. *Perception* 22: 1389–1402, 1993.
- Curcio CA, Sloan KR, Kalina RE, Hendrickson AE.** Human photoreceptor topography. *J Comp Neurol* 292: 497–523, 1990.
- Daniel PM, Whitteridge D.** The representation of the visual field on the cerebral cortex in monkeys. *J Physiol* 159: 203–221, 1961.
- DeYoe EA, Carman GJ, Bandettini P, Glickman S, Wieser J, Cox R, Miller D, Neitz J.** Mapping striate and extrastriate visual areas in human cerebral cortex. *Proc Natl Acad Sci USA* 93: 2382–2386, 1996.
- Dougherty RF, Koch VM, Brewer AA, Fischer B, Modersitzki J, Wandell BA.** Visual field representations and locations of visual areas V1/2/3 in human visual cortex. *J Vis* 3: 586–598, 2003.
- Dow BM, Snyder AZ, Vautin RG, Bauer R.** Magnification factor and receptive field size in foveal striate cortex of the monkey. *Exp Brain Res* 44: 213–228, 1981.
- Dow BM, Vautin RG, Bauer R.** The mapping of visual space onto foveal striate cortex in the macaque monkey. *J Neurosci* 5: 890–902, 1985.
- Duncan RO, Boynton GM.** Cortical magnification within human primary visual cortex correlates with acuity thresholds. *Neuron* 38: 659–671, 2003.
- Engel SA, Rumelhart DE, Wandell BA, Lee AT, Glover GH, Chichilnisky EJ, Shadlen MN.** fMRI of human visual cortex. *Nature* 369: 525–527, 1994.
- Fiorani M Jr, Gattass R, Rosa MG, Sousa AP.** Visual area MT in the Cebus monkey: location, visuotopic organization, and variability. *J Comp Neurol* 287: 98–118, 1989.
- Fischer B, Modersitzki J.** Fast inversion of matrices arising in image processing. *Num Algorithms* 22: 1–11, 1999.
- Fritsches KA, Rosa MG.** Visuotopic organisation of striate cortex in the marmoset monkey (*Callithrix jacchus*). *J Comp Neurol* 372: 264–282, 1996.
- Gattass R, Sousa AP, Rosa MG.** Visual topography of V1 in the Cebus monkey. *J Comp Neurol* 259: 529–548, 1987.
- Gattass R, Nascimento-Silva S, Soares JG, Lima B, Jansen AK, Diogo AC, Farias MF, Botelho MM, Mariani OS, Azzi J, Fiorani M.** Cortical visual areas in monkeys: location, topography, connections, columns, plasticity and cortical dynamics. *Philos Trans R Soc Lond B Biol Sci* 360: 709–31, 2005.
- Holmes G.** Disturbances of vision by cerebral lesions. *Br J Ophthalmol* 2: 353–384, 1917.
- Horton JC, Hedley-Whyte ET.** Mapping of cytochrome oxidase patches and ocular dominance columns in human visual cortex. *Philos Trans R Soc Lond B Biol Sci* 304: 255–272, 1984.
- Horton JC, Hoyt WF.** The representation of the visual field in human striate cortex. A revision of the classic Holmes map. *Arch Ophthalmol* 109: 816–824, 1991a.

- Horton JC, Hoyt WF.** Quadrantic visual field defects. A hallmark of lesions in extrastriate (V2/V3) cortex. *Brain* 114: 1703–1818, 1991b.
- Hubel DH, Wiesel TN.** Uniformity of monkey striate cortex: a parallel relationship between field size, scatter, and magnification factor. *J Comp Neurol* 158: 295–305, 1974.
- Inouye T.** *Die Sehstörungen bei Schussverletzungen der kortikalen Sehsphäre nach Beobachtungen an Verwundeten der letzten japanischen Kriege.* Leipzig, Germany: W Engelmann, 1909. [In German, translated by M Glickstein and M. Fahle. *Brain* 123: *Special Suppl* 1–101, 2000].
- Kaplow WK, Schwartz EL.** Measuring mean and Gaussian curvature on triangulated brain surfaces: the differential geometry of macaque striate cortex. *Invest Ophthalmol Vis Res Suppl* 26: 164, 1986.
- LeVay S, Connolly M, Houde J, Van Essen DC.** The complete pattern of ocular dominance stripes in the striate cortex and visual field of the macaque monkey. *J Neurosci* 5: 486–501, 1985.
- LeVay S, Hubel DH, Wiesel TN.** The pattern of ocular dominance columns in macaque visual cortex revealed by a reduced silver stain. *J Comp Neurol* 159: 559–576, 1975.
- Levi DM, Klein SA, Aitsebaomo P.** Detection and discrimination of the direction of motion in central and peripheral vision of normal and amblyopic observers. *Vision Res* 24: 789–800, 1984.
- McKee SP, Nakayama K.** The detection of motion in the peripheral visual field. *Vision Res* 24: 25–32, 1984.
- Mitchell DE, Freeman RD, Westheimer G.** Effect of orientation on the modulation sensitivity for interference fringes on the retina. *J Opt Soc Am* 57: 246–249, 1967.
- Myerson J, Manis PB, Miezin FM, Allman JM.** Magnification in striate cortex and retinal ganglion cell layer of owl monkey: a quantitative comparison. *Science* 198: 855–857, 1977.
- Østerberg GA.** Topography of the layer of rods and cones in the human retina. *Acta Ophthalmol* 13 *Suppl* 6: 1–97, 1935.
- Pelli DG.** The VideoToolbox software for visual psychophysics: transforming numbers into movies. *Spat Vis* 10: 437–442, 1997.
- Polimeni JR, Balasubramanian M, Schwartz EL.** Multi-area visuotopic map complexes in macaque striate and extra-striate cortex. *Vision Res* 46: 3336–3359, 2006.
- Press WA, Brewer AA, Dougherty RF, Wade AR, Wandell BA.** Visual areas and spatial summation in human visual cortex. *Vision Res* 41: 1321–1332, 2001.
- Rosa MG, Tweedale R.** Visual areas in lateral and ventral extrastriate cortices of the marmoset monkey. *J Comp Neurol* 422: 621–651, 2000.
- Rosa MG, Tweedale R.** Brain maps, great and small: lessons from comparative studies of primate visual cortical organization. *Philos Trans R Soc Lond B Biol Sci* 360: 665–691, 2005.
- Rovamo J, Virsu V.** An estimation and application of the human cortical magnification factor. *Exp Brain Res* 37: 495–510, 1979.
- Rovamo J, Virsu V.** Isotropy of cortical magnification and topography of striate cortex. *Vision Res* 24: 283–286, 1984.
- Schwartz EL.** The development of specific visual connections in the monkey and the goldfish: outline of a geometric theory of receptotopic structure. *J Theor Biol* 69: 655–683, 1977.
- Schwartz EL.** Cortical mapping and perceptual invariance: a reply to Cavanagh. *Vision Res* 23: 831–835, 1983.
- Schwartz EL.** Computational studies of the spatial architecture of primate visual cortex: columns, maps, and protomaps. *Cereb Cortex* 10: 359–411.
- Sereno MI, Dale AM, Reppas JB, Kwong KK, Belliveau JW, Brady TJ, Rosen BR, Tootell RB.** Borders of multiple visual areas in humans revealed by functional magnetic resonance imaging. 268: 889–893, 1995.
- Shipp S, Zeki S.** The functional organization of area V2, II: the impact of stripes on visual topography. *Vis Neurosci* 19: 211–231, 2002.
- Slotnick SD, Klein SA, Carney T, Sutter EE.** Electrophysiological estimate of human cortical magnification. *Clin Neurophysiol* 112: 1349–1356, 2001.
- Stensaas SS, Eddington DK, Dobelle WH.** The topography and variability of the primary visual cortex in man. *J Neurosurg* 40: 747–755, 1974.
- Talbot SA, Marshall WH.** Physiological studies on neural mechanisms of visual localization and discrimination. *Am J Ophthalmol* 24: 1255–1263, 1941.
- Toet A, Levi DM.** The two-dimensional shape of spatial interaction zones in the parafovea. *Vision Res* 32: 1349–1357, 1992.
- Tootell RB, Dale AM, Sereno MI, Malach R.** New images from human visual cortex. *Trends Neurosci* 19: 481–489, 1996.
- Tootell RB, Switkes E, Silverman MS, Hamilton SL.** Functional anatomy of macaque striate cortex. II. Retinotopic organization. *J Neurosci* 8: 1531–1568, 1988.
- Tusa RJ, Palmer LA, Rosenquist AC.** The retinotopic organization of area 17 (striate cortex) in the cat. *J Comp Neurol* 177: 213–235, 1978.
- Torgerson WS.** Multidimensional scaling. I. Theory and method. *Psychometrika* 17: 401–419, 1952.
- Tyler CW.** The symmetry magnification function varies with detection task. *J Vision* 1: 137–44, 2001.
- Tyler CW, Likova LT, Kontsevich LL, Schira M, Wade AR.** Enhanced concepts of occipital retinotopy. *Current Med Imag Rev* 1: 319–329, 2005.
- Van Essen DC, Lewis JW, Drury HA, Hadjikhani N, Tootell RB, Bakircioglu M, Miller MI.** Mapping visual cortex in monkeys and humans using surface-based atlases. *Vision Res* 41: 1359–1378, 2001.
- Van Essen DC, Newsome WT, Maunsell JH.** The visual field representation in striate cortex of the macaque monkey: asymmetries, anisotropies, and individual variability. *Vision Res* 24: 429–448, 1984.
- Wertheim Th.** Über die indirekte Sehschärfe. *Zeitschrift für Psychol Physiol Sinnesorgane* 7: 172–187, 1894.
- Westheimer G.** Meridional anisotropy in visual processing: implications for the neural site of the oblique effect. *Vision Res* 43: 2281–2289, 2003.
- Yap YL, Levi DM, Klein SA.** Peripheral hyperacuity: isoeccentric bisection is better than radial bisection. *J Opt Soc Am A* 4: 1562–1567, 1987.
- Zegarra-Moran O, Geiger G.** Visual recognition in the peripheral field: letters versus symbols and adults versus children. *Perception* 22: 77–90, 1993.

## Supplementary Material

### Individual Magnification Functions to Investigate Intersubject Variability

The study by Dougherty *et al.* (2003) reports a high degree of intersubject variability in V1 area (up 2.4 times; see also Stensaas *et al.*, 1974; Duncan and Boynton, 2003). We confirm these results: the biggest V1 in our sample has 2.3 times the area of the smallest (the cortical area is proportional to  $k^2$ , so compare subject 4 with  $k = 26.1$  and subject 6 with  $k = 17.1$ ). However, as is illustrated in Figure S1, the two subjects basically differ in overall size and are well fit by functions with the same value for  $a$  as the group average in their V1 organization.



	s1	s2	s3	s4	s5	s6	s7	s8	mean
$k$ [mm]	23.5	23.6	21.0	26.1	19.3	17.1	18.0	20.8	21.1
mean err [mm/deg]	0.63	1.52	1.34	1.85	0.97	1.60	1.93	1.07	1.36
expl. variance [%]	98	94	97	98	97	86	91	99	95
HM [mm]	52.7	52.9	47.0	58.5	43.3	38.3	40.3	46.6	47.5
area [mm <sup>2</sup> ]	1838	1853	1467	2267	1239	973	1078	1439	1519

Table S1. Quality of the fits shown in Figure S1. We also calculated the length of the horizontal meridian (HM) and the amount area of cortex V1 from 0.5-12 correspond to these values. The variance in surface between subject 4 and subject 6 is big (2.3 times), whereas the difference in length of the horizontal meridian is only 1.5 times.

### **Length of Meridians to Investigate the Flatness of V1 and V2**

The models presented in this paper all assume that human V1 and V2 are essentially flat. If V1 is flat and approximates the matches the observed shape this requires that the length of the isopolar meridians increases progressively with their angular position. (Note that we use the terms ‘meridian’ and ‘isopolar meridian’ to refer to the cortical representation of a retinal meridian if it is being discussed in the context of a cortical map.) We measured the lengths of a set of different meridians in the three dimensional cortical manifolds and averaged them across subjects. The results of these measurements are plotted in Figure S2. Figure S2a confirms that average lengths of the meridians in V1 increase gradually with polar position. Figure S2b shows that there is little difference between the upper and the lower visual field meridians, implying a symmetric representation on human visual cortex. Figure S2c,d test the quantitative predictions of the original model of Balasubramanian et al. (2002), and of our Parametric-2D-Shear modification of this model, respectively. Note that the both models fit to the V1 meridian values within the experimental error, but for V2 and V3 the model by Balasubramanian et al. largely deviates from the measured results. This deviation is reduced by our model, but we suggest that, for an adequate match V2v and V2h can be modeled only if V2 has intrinsic curvature.

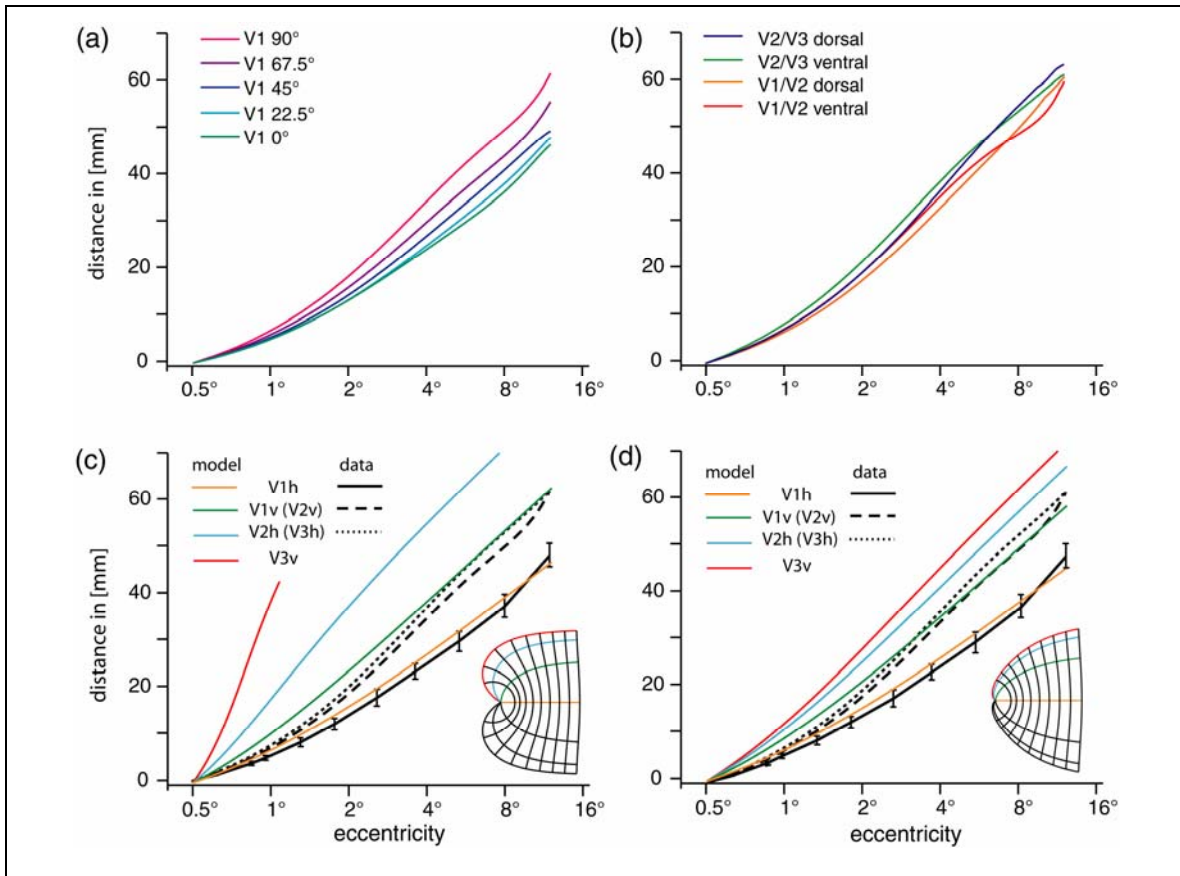


**Figure S2:** Isopolar lengths. **a)** Within V1 the measured length of the isopolar lines increases gradually with polar angle (here averaged between upper and lower visual field). For simplicity, we do not plot error bars here; the errors are comparable to those for V1 horizontal meridian data, in c. **b)** There was no significant difference between the upper and lower visual field. **c)** Modeled isopolar lines as predicted by Balasubramanian et al. (2002) are in color; the measured data in black. Within V1 the modeled lengths match the prediction; however for the horizontal meridian in V2/V3 the measured length is smaller than the prediction. **d)** Predictions of the Parametric-2D-shear model. The deviation is reduced, but the length prediction for V2/V3 is still larger than the measurement values, suggesting that V2 has intrinsic curvature.

### Model Fits in 2D.

We have proposed our models based on the theoretical principle of equal-area mapping along the meridians. We compared various properties of these models with results from undistorted measurements, and these results encouraged us to make a flat reconstruction of V1 (see Figure 8), the approach that had been taken by Schwartz. Here we compare the fit of the original Schwartz Model (or its variants) with the two new

equal-area models we propose to improve the fits. Each of these three model families can be specified either in a monopole version (parameters  $a$ ,  $k$  and global shear) or in a dipole version (with an additional pole in the periphery governed by parameter  $b$ ). Although it is clear that when modeling V1 as a whole the dipole parameter  $b$  is needed to describe the reconvergence at the periphery, our data cover only the central part of the visual field. Accordingly we have insufficient information to fit  $b$ , and the improvement of the fit provided by  $b$  is negligible (See Figure S3 last two rows). The global shear parameter leads to significant improvements of the model fits, although at the cost of changing the values for  $a$  and  $k$ , thereby making a comparison with linear magnification data fitted to eq. 1 impossible. Our fits also show that each of the models we propose performs consistently better than the original Schwartz Model. The difference is most significant when the global shear parameter is removed. Here it is worth noticing that a (rotational) global shear of 0.72 (or  $\alpha_l$  in the terminology of Balasubramanian et al., 2002), reduces the areal anisotropy between the horizontal and the vertical meridians from a factor of 2 (with global shear = 1) to a factor of only 1.16 (with global shear = 0.72). Thereby the rotational shear factor  $\alpha_l$  not only changes outer shape of the model, but also the intrinsic organization (only for the variants of the Schwartz model, but not for our models).

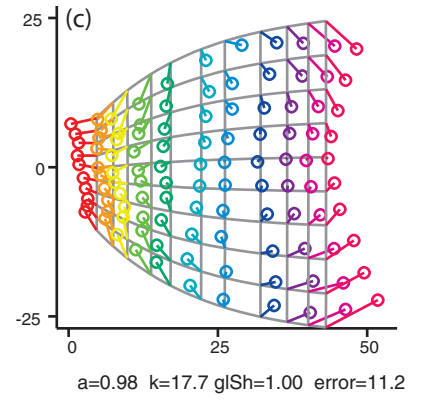
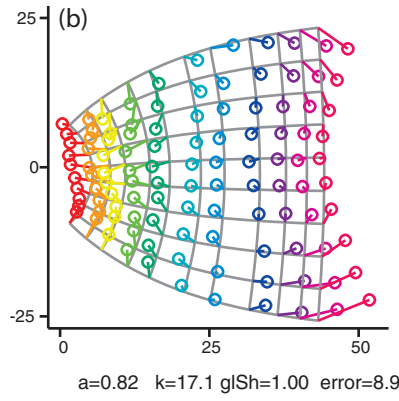
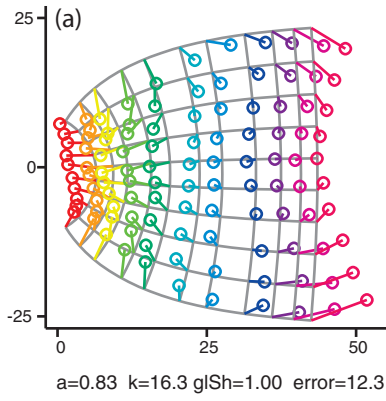
**Figure S3 (next page).** Results of the model fit. The models are sorted in columns, the parameter variations in rows. The gray grids depict the models, the colored circles are our data, and the colored lines connect the modeled and the measured positions. The errors are the mean variance in  $mm^2$ . Rows 1 and 2 depict the results for fitting monopole versions of the models. Row 1 (a-c) shows the fits with  $k$  and  $a$  as free parameters, testing the simplest versions of the models discussed in this paper. Only the results of this row are comparable with magnification expressed in eq. 1, and the values of  $a$  and  $k$  providing the best fit are similar to the values reported in Figure 1. In this row the Parametric-2D-Shear model (b) clearly provides the best fit. The second row (d-f) depicts the fits after introducing an additional parameter: *global shear*. It is worth noting that this parameter leads to a local anisotropy throughout the whole visual field. Here the Divisory Model provides an excellent fit, resulting in a mean variance of only  $2.8 mm^2$ . However, neither of the monopole models can describe the strong bend ('fishtail') of our data at eccentricities of 10 and  $12^\circ$ . The dipole models could provide this curvature in principle, but would require a very small  $b$ . Row 3 (g-i) depicts the results of a dipole model where  $b$  is not fitted but fixed at  $90^\circ$ . Finally, Row 4 (j-l) shows the result of the models if all parameters are free. These fits result in very small estimations of  $b$ . However it is worth noting that the additional parameter  $b$  results in small improvements of the fit, and in estimations of  $a$  and  $k$  rather different from those obtained by fits to equation 1.

Schwartz/Balasubramanian

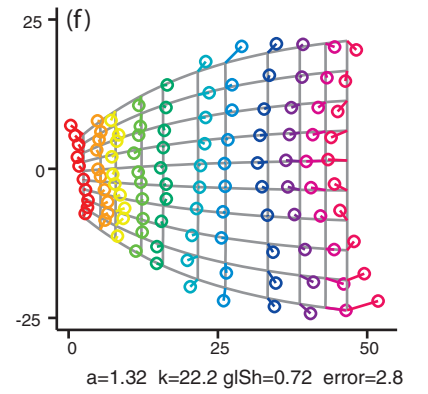
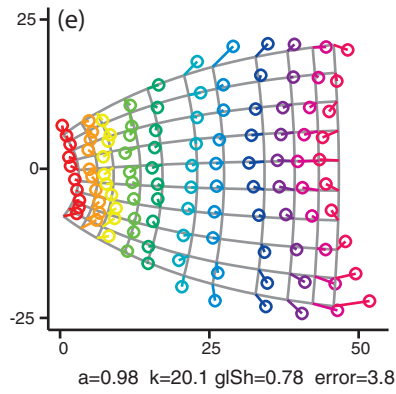
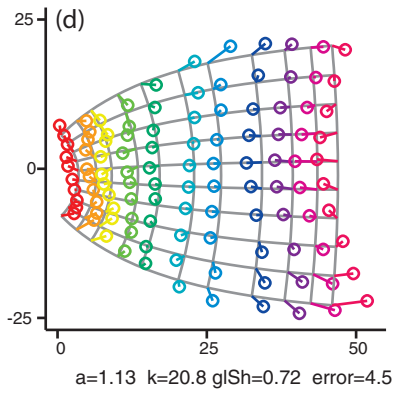
Parametric-2D-Shear

Divisory

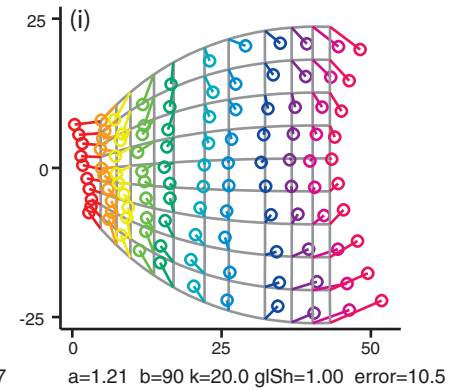
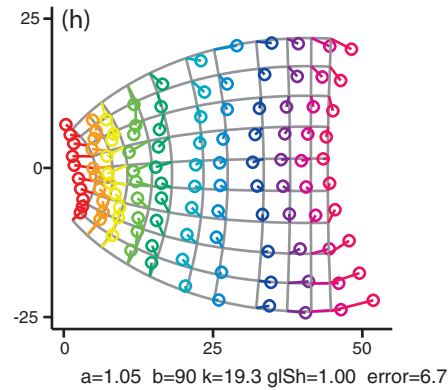
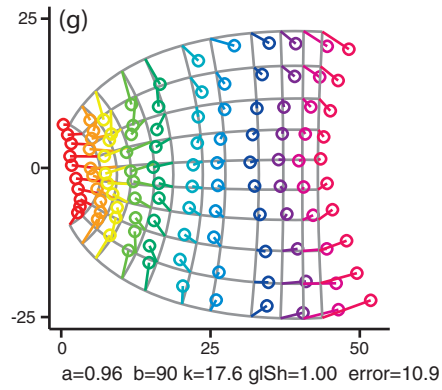
Monopole fitted a, k



Monopole, fitted a, k, global shear



Dipole, fitted, a, k



Dipole, fitted a, b, k, global shear

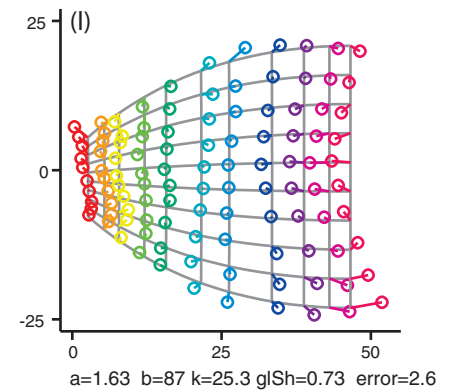
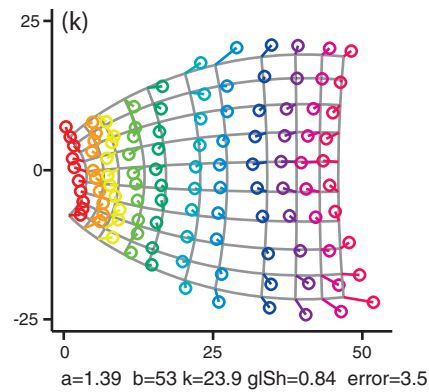
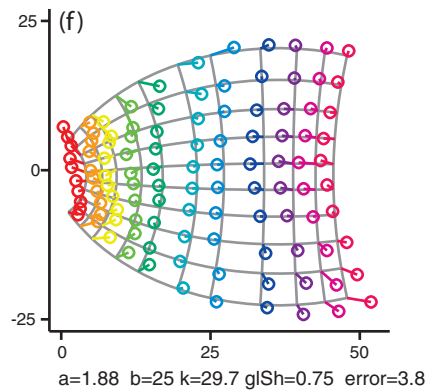


Figure S3

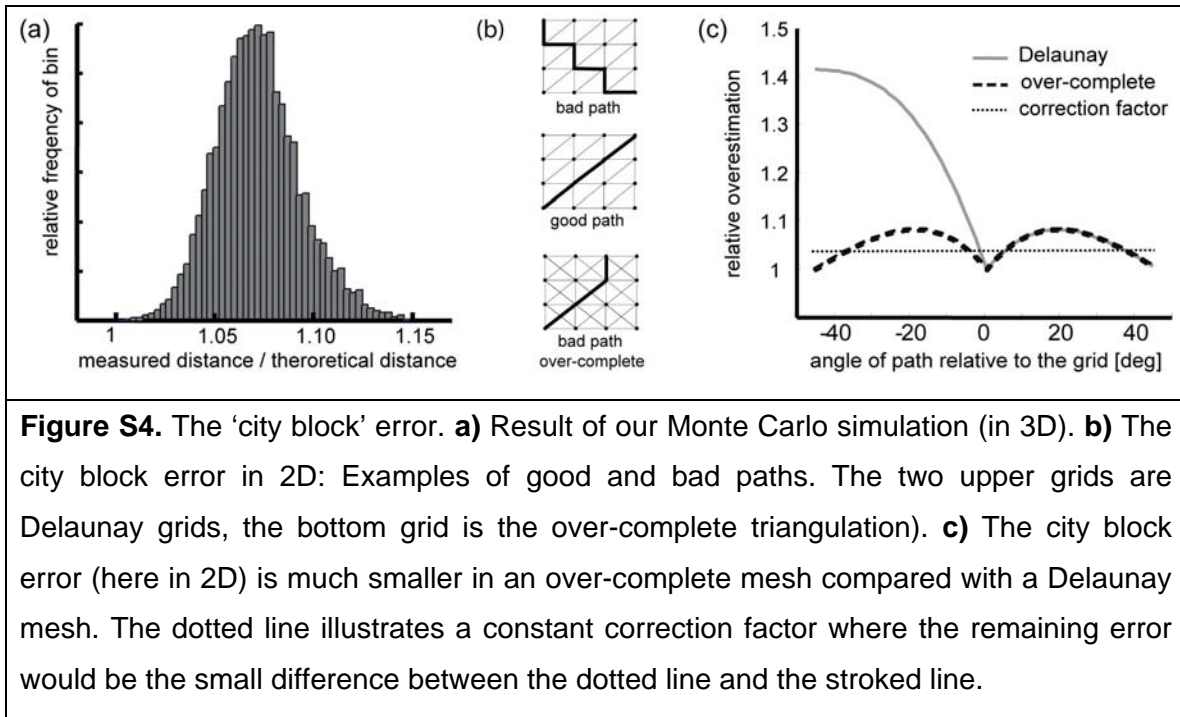
### Measuring Distances on a 3D Mesh

Measuring distances along a folded 3D manifold (the cortex surface) is an important element of this publication. The results reported in Figures 6, 7, 8, S2 and S3 (but not those in figure 2,3 and S1) rely on the accurate performance of this task. It is important to specify that we perform this task based on a representation of the human brain in a voxel space (resolution 1x1x1 mm). This starts with the 3D anatomical measurement of gray values from the T1-weighted anatomical measurements. By segmenting the brain each of these voxels is identified to be either white matter, gray matter or cerebrospinal fluid. Based on this representation, a mesh reconstruction of the gray-white boundary is calculated. It is in this mesh that we measure the distances provided in this paper. The nodes of this mesh are still restricted to the grid introduced by the voxelated representation of measured human cortex.

We used the Dijkstra algorithm (see Skiena, 1990) to estimate the shortest path (distance) between two nodes in questions. Measuring distances along a rectangular grid (in 2 or 3 dimensions) is subject to the ‘city block error’ (or ‘Manhattan Distance’, error described by Hermann Minkowski 1864-1909). This basically means that in a rectangular grid the distance one has to travel between any two points can be as short as the Euclidian distance or up to  $\sqrt{2}$  times the Euclidian distance (for diagonals). Adding one set of diagonals (for example a Delaunay mesh) to the grid reduces the mean error but not the maximum error (Figure S4b,c). Adding both diagonals between neighboring points (making an over-complete triangulated mesh) reduces the maximum error to  $\frac{1+\sqrt{2}}{\sqrt{5}}$

(Figure S4b,c). In a 3D manifold these ranges are higher (see Figure S4a) but comparable. To test how these errors are distributed we performed a Monte Carlo simulation. We measured the distance between random positions on a mesh representation of a sphere using the Dijkstra algorithm and compared the measured distances with the theoretical distances on an ideal sphere (which incorporates all possible directions and curvatures through the sampled space, yet represents a simple geometrical object where distances are well understood), thereby simultaneously testing all the methodological errors of our procedure. The results of this are presented in Figure S4a. There was a mean overestimation of  $1.075 \pm 0.021$  (standard deviation), while the

distribution is well described by a normal distribution, and did not depend on the diameter of the sphere.



Skiena S (1990) *Implementing Discrete Mathematics Combinatorics and Graph Theory with Mathematica*. Addison-Wesley, Reading, MA, pp. 225–227.